

1 Effects of Sea Surface Temperature on Tropical Shallow
2 Circulation Strength

3 Brittany D. Dygert and Dennis L. Hartmann

4 ¹Department of Atmospheric and Climate Science, University of Washington, Seattle, Washington 98195

5 Key Points:

- 6 • Both warming the average sea surface temperature and increasing its gradient in-**
- 7 crease the strength of the shallow circulation.**
- 8 • Warming the sea surface temperature strengthens shallow circulations by enhanc-**
- 9 ing shallow convection.**
- 10 • Increasing the sea surface temperature gradient strengthens shallow circulations**
- 11 by enhancing longwave cooling.**

12 **Abstract**

13 Shallow circulations in the tropics are related to the sea surface temperature dis-
 14 tribution, longwave cooling above the boundary layer, and shallow convection in both
 15 observations and idealized models. To understand the influences sea surface tempera-
 16 ture has on the shallow circulation strength, fixed sea surface temperature distributions
 17 are applied in experiments with a general circulation model. The experiments are de-
 18 signed to distinguish the effects of mean sea surface temperature from those of sea sur-
 19 face temperature gradients. In these simulations, a large-scale, deep circulation devel-
 20 ops connecting the coldest to hottest SSTs. Experiments with sufficiently large sea sur-
 21 face temperature mean or range also exhibit a distinct shallow cell above the boundary
 22 layer. We find that warming the mean sea surface temperature increases the strength
 23 of these shallow circulations primarily by increasing shallow convection, while increas-
 24 ing the sea surface temperature gradient enhances shallow circulation strength primar-
 25 ily by enhancing boundary layer longwave cooling.

26 **Plain Language Summary**

27 In the tropics, rising motions are driven by latent heat release associated with rain-
 28 fall over warmer parts of the ocean. These regions of rising motion are connected to re-
 29 gions of sinking motion where the atmosphere is cooled by radiative emission. Atmospheric
 30 winds connect the regions of rising and sinking motion, and these circulations play an
 31 important role in weather and climate. Some of these circulations are deep and extend
 32 from the surface to just below the tropopause, and some are shallow, such that the ris-
 33 ing and sinking motion and associated winds are limited to the lower part of the atmo-
 34 sphere. We perform simulations with a global model to explore the effect of mean sea
 35 surface temperature (SST) and horizontal gradients of SST on the relative strength of
 36 the shallow and deep circulations. We find that the strength of the shallow circulation
 37 increases both with the mean SST and the horizontal gradient of SST, but for different
 38 reasons. The gradient of SST more strongly affects the radiative cooling in the region
 39 of sinking motion, while the mean SST increases the strength of the shallow latent heat-
 40 ing in the region of rising motion.

41 **1 Introduction**

42 Understanding the atmospheric circulation in the tropics and its interaction with
 43 convection and radiation is critical to the global radiation budget and climate sensitiv-
 44 ity (Bony et al., 2015; Dong et al., 2019; Armour et al., 2024). While the predominant
 45 view of the tropical circulation envisions a single deep cell, shallow circulations are known
 46 to occur in the tropics in both observations and reanalysis datasets (Schulz & Stevens,
 47 2018); the shallow meridional circulation (SMC) on the flanks of the intertropical con-
 48 vergence zone (ITCZ) in the East Pacific is particularly prominent (Zhang et al., 2004,
 49 2008; Huaman et al., 2022). These shallow circulations are characterized by strong re-
 50 turn flow above the boundary layer and are often identified in regions with strong sea
 51 surface temperature gradients (Zhang et al., 2004). Fläschner et al. (2018) have shown
 52 that shallow circulations can have a strong effect on the distribution of precipitation and
 53 its response to warming in climate models.

54 Several studies have investigated the mechanisms underlying these shallow circu-
 55 lations. One potential driver of this shallow circulation is boundary layer pressure gra-
 56 dients created by SST gradients, as in a sea-breeze (Nolan et al., 2007; Lindzen & Nigam,
 57 1987). Other studies find boundary layer radiative cooling to be the best indicator of shal-
 58 low circulation strength (Nishant et al., 2016; Naumann et al., 2017). Naumann et al.
 59 (2017) specifically address the direct impact of sea surface temperature gradients and
 60 longwave cooling, and find that longwave cooling is the primary driver. While they found

61 that SST gradients were not strong enough to explain the shallow circulation strength
 62 through their direct impact on boundary layer pressure gradients, they acknowledge that
 63 the longwave cooling increases in experiments with stronger SST gradients due to the
 64 effect of SST gradients on the relative humidity distribution. Moving to a smaller scale,
 65 Janssens et al. (2024) find that, at the mesoscale, shallow convection is the primary driver
 66 of tropical shallow circulations. In their study the SST gradients are relatively weak, and
 67 they do not speculate on the potential effects of SST on shallow convection. Discrepan-
 68 cies between these studies are likely partially a product of scale, with SST gradient driven
 69 flows representing the largest scale. Convection and circulation are also closely tied in
 70 the tropics at larger scales, through a combination of surface moisture convergence and
 71 convective instability (Tomassini, 2020; Back & Bretherton, 2009).

72 Several prior studies using a simplified mock-Walker simulation setup designed to
 73 emulate the overturning circulation along the equator have found that a double-cell struc-
 74 ture, in which both shallow and deep circulations are present, develops in these simu-
 75 lations (Grabowski et al., 2000; Larson & Hartmann, 2003; Yano et al., 2002; Lutsko &
 76 Cronin, 2018). These studies focus on explaining the development of the shallow circu-
 77 lation as primarily being driven by radiative cooling in the subsiding region or shallow
 78 convective heating in the rising portion of the shallow cell. Diagnostically, it is difficult
 79 to say which of these factors is the primary control on the development of shallow cir-
 80 culations, as both are required to sustain a shallow circulation cell energetically. This
 81 problem has recently been addressed in the context of mock-Walker circulations in a con-
 82 viction permitting model by Lutsko and Cronin (2024). They find that a double-cell cir-
 83 culation always develops in this model when surface temperatures are higher than about
 84 300 K, and that the development of the double-cell structure is encouraged by SST gra-
 85 dients. Adding moisture to the subsiding region or fixing the radiative cooling reduces
 86 the radiative cooling mechanism and moves the development of the double-cell structure
 87 to a higher mean temperature closer to 305 K. This suggests that a mechanism other than
 88 radiative cooling also encourages a double-cell structure with a strong shallow circula-
 89 tion when the surface temperature is warm.

90 Many previous studies have investigated the relationship between SST gradients
 91 and circulation. These studies vary from more general interactions between sea surface
 92 temperature and circulation strength, to specific effects on the top and bottom heavi-
 93 ness of the distribution (Lindzen & Nigam, 1987; Sobel & Neelin, 2006). Back and Brether-
 94 ton (2009) use a linear mixed layer model to find that sea surface temperature gradients
 95 lead to shallow convergence and convection.

96 Our goal here is to better understand the comparative roles of mean SST and SST
 97 gradients in generating shallow circulations in a tropical context. To do this we use a
 98 simplified framework of a global climate model with uniform insolation and no rotation,
 99 emulating a global tropical world. We use fixed SST simulations and vary the mean SST
 100 and the SST gradient in the domain and compare the shallow versus deep circulations
 101 in a suite of experiments in which the mean SST and SST gradient are varied indepen-
 102 dently. We diagnose the relative roles of radiative cooling and convective heating in driv-
 103 ing shallow circulations. We find that SST gradients are important in driving shallow
 104 circulations and that the primary energetic support for these shallow circulations is ra-
 105 diative cooling. As the mean SST is increased, however, we see an increasing role for shal-
 106 low convection in driving shallow circulations. We diagnose the reasons for the increased
 107 shallow convection with a convective plume model.

108 The model and experimental design are described in Section 2. The circulation re-
 109 sponse to mean SST and SST gradient are described in Section 3.1. The effects of long-
 110 wave cooling on the circulations are described in Section 4. Diagnosis and interpreta-
 111 tion of the effect of shallow convection on shallow circulation strength are given in Sec-
 112 tion 5. A summary is provided in Section 6.

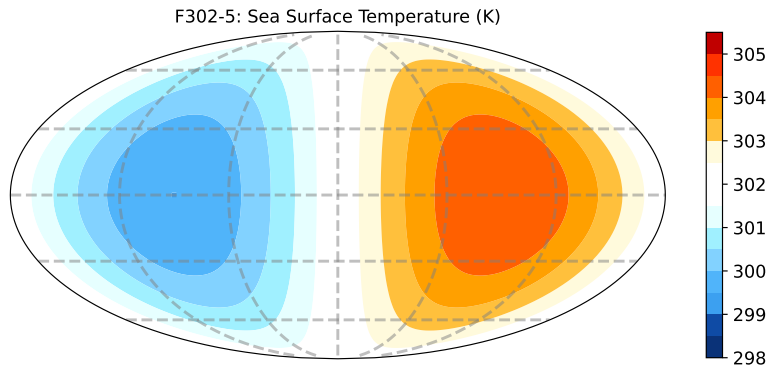


Figure 1. Example of prescribed sea surface temperature (K) in latitude and longitude for F302-5, or the case with a global mean SST of 302 K and a range of 5 K.

2 Model and Experiments

These experiments use Geophysical Fluid Dynamics Laboratory's (GFDL) AM2.1 (Anderson et al., 2004). We use a grid with 2 by 2.5 degree horizontal resolution and 32 vertical levels. We simplify the model by using uniform insolation, no rotation, and prescribed SST. The experiments are spun up until equilibrium, and extended for two decades after equilibrium.

The intention of these experiments is to evaluate the effect of changes in both mean SST and SST range. We prescribe SST with a spatial distribution of wavenumber 1 and mean of 299, 302, 303.5, and 305 K. Experiments using these mean SSTs are run with SST ranges of 2.5, 5, 7.5, 10 and 15 K. Each case is named by its global mean SST and SST range. For example, the SST for the case F302-5, is shown in Figure 1, has a global mean SST of 302 K and a SST range of 5 K.

Moist convection, and particularly the height of convection, is central to these experiments. In AM2.1, this is parameterized using the Relaxed Arakawa-Schubert (RAS) scheme, with the addition of the Tokioka parameter to constrain the activation of deep convection in updrafts without a sufficiently large lateral entrainment rate (Moorthi & Suarez, 1992; Tokioka et al., 1988). AM2.1 treats convection as detraining plumes, where updraft level of detainment determines whether the convection is classified as shallow, deep, or in between. Shallow convection detrains below 800 hPa and deep convection detrains above 500 hPa. Parameter values are linearly interpolated for detrainment levels in between. When we refer to shallow convection in this paper, we are also including midlevel convection that falls into the intermediate range of parameterizations.

3 Circulation

3.1 Streamfunction

The circulation can be visualized through a mass streamfunction calculated for each case, as shown in Figure 2. Here, we organize the circulation in column relative humidity (CRH) area space, such that the stream function flows from dry to moist regions. The

140 CRH area fraction is then given by

$$\Phi_A(CRH) = \int_0^{CRH} f_A dCRH \quad (1)$$

141 where f_A is the fraction of the total area of the globe that falls within the CRH bin. The
142 streamfunction is then given by

$$\Psi(\Phi_A, p) = \frac{A_E}{g} \int_0^{\Phi_A} \omega(p) d\Phi'_A \quad (2)$$

143 where A_E is the global area, g is the gravitational constant, and ω is the vertical velocity
144 in Pa/s at a specific pressure level, p .

145 This is the same expression used in Hartmann and Dygert (2022) with CRH area
146 fraction in place of SST area fraction. CRH was chosen here because in the cases with
147 small SST gradients the circulation is not well organized by SST, and CRH better cap-
148 tures the contrast between regions of rising and sinking motion. In those cases with larger
149 SST contrast, using CRH area fraction or SST area fraction yield similar results.

150 In Figure 2 the mean SST increases from left to right and the SST contrast increases
151 from bottom to top. In all cases, as the global mean SST increases the upper cell weak-
152 ens and the shallow cell strengthens. The weakening of the upper cell is consistent with
153 studies finding that the tropical overturning atmospheric circulation will weaken under
154 warming, primarily because of the increasing dry static stability (Knutson & Manabe,
155 1995; Vecchi & Soden, 2007). Figure 2 also shows that as the range of SST increases from
156 bottom to top, the shallow circulation strengthens and the circulation takes on a more
157 distinct double cell structure. As the SST range increases, the upper cell tends to shrink
158 toward higher CRH such that the upper cell is strong only over the highest CRH area
159 fractions. So increasing the global mean SST and the SST range both increase the strength
160 of the shallow cell and the double-cell structure of the circulation.

161 As shown in the bottom row of Figure 2, the circulation in the cases with an SST
162 range of 2.5 K is particularly top heavy and does not have a strong shallow cell. The weak
163 SST gradient is not sufficient to produce strong large-scale organization, given the in-
164 ternal variability of the simulations, and these cases are the least consistent with the oth-
165 ers. Even so, the upper cell still rises and weakens with warming, and the circulation starts
166 to show a distinct double cell structure by the warmest experiment, F305-2.5.

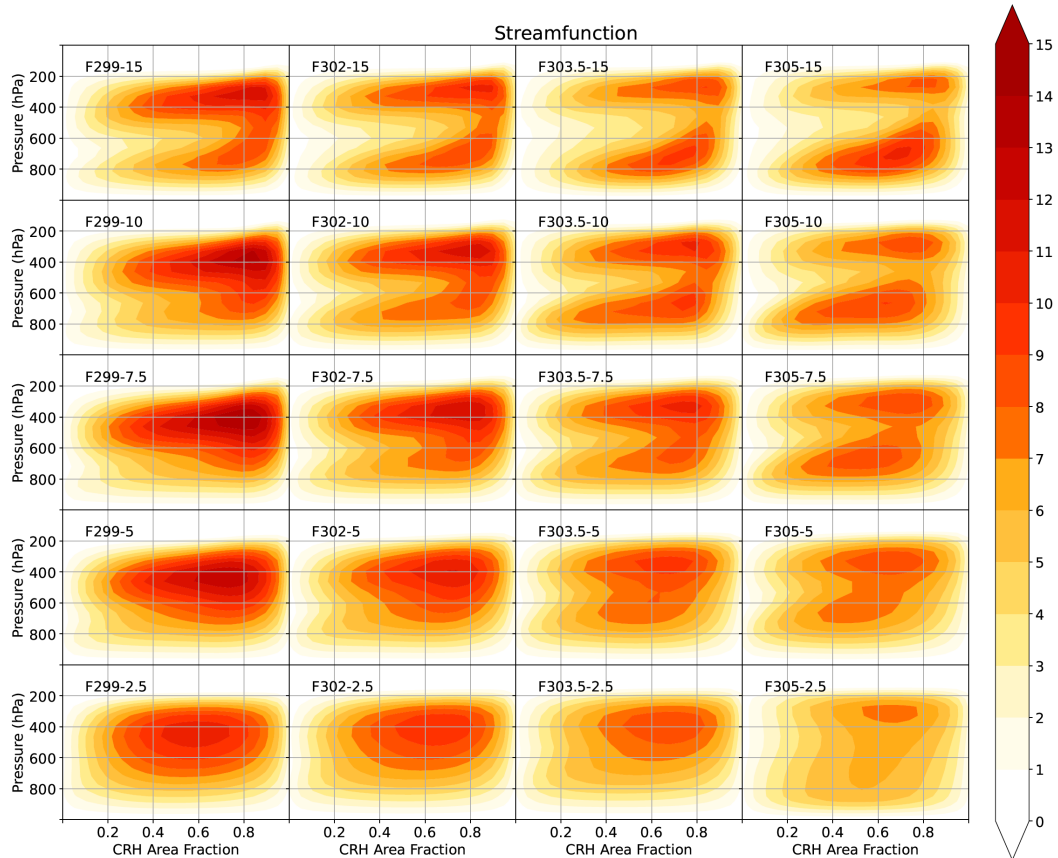


Figure 2. Streamfunction for each case shown in pressure (hPa) and column relative humidity (CRH) area space (%). The global mean SST of each case increases from left to right, and the SST range increases from bottom to top.

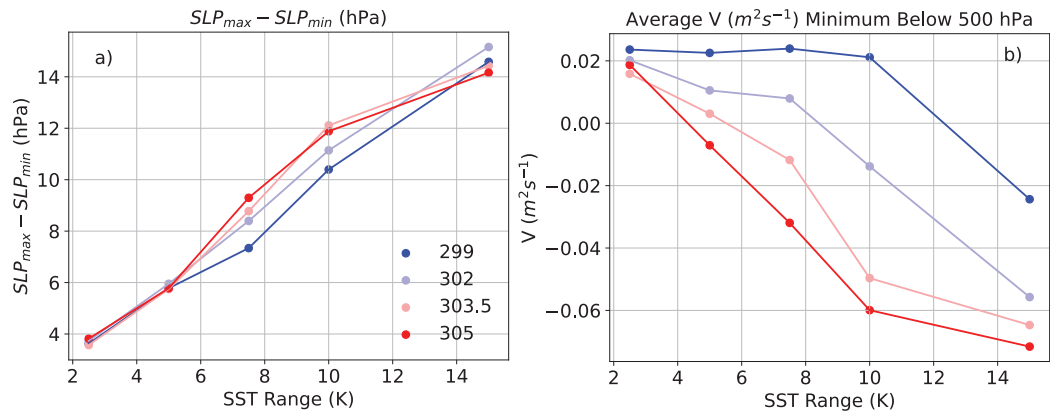


Figure 3. a) Surface pressure difference from minimum to maximum CRH as a function of SST contrast for each mean temperature. b) minimum horizontal area velocity (V) averaged over all CRH values for each mean temperature.

167 Alternative visualizations of the circulation can be found in the Supplemental Material:
 168 including an example of the streamfunction in longitude space (Figure S1) as well
 169 as an equivalent figure showing the vertical velocity response of each experiment directly
 170 (Figure S2). Further detail on the response of the circulation to SST is shown in Fig-
 171 ure 3. Figure 3a shows that as the SST contrast is increased, the pressure contrast be-
 172 tween driest (coldest) and wettest (warmest) portions of the domain increases linearly,
 173 with relatively modest sensitivity to mean temperature. This might be expected from
 174 the relation of SST to surface pressure predicted by hydrostatic considerations (Lindzen
 175 & Nigam, 1987). One would expect these increasing surface pressure gradients to drive
 176 a stronger near-surface flow toward warmer SST.

177 It is important to note here that as the SST gradient or mean SST increases and
 178 the lower cell strengthens, the circulation also deepens, particularly in the higher CRH
 179 value regions of the circulation. The idealized nature of these experiments allow for a
 180 larger-scale than is seen in nature. Zhang et al. (2004) characterize the Shallow Merid-
 181 ional Circulation as having a strong return flow around 600 hPa. This more closely re-
 182 sembles the lower CRH area fraction regions of these experiments. In these experiments,
 183 we refer to the strength of this lower cell as the strength of the shallow circulation.

184 A more direct measure of the relative strength of the shallow circulation is shown
 185 in Figure 3b. Here, we show an effective "horizontal area velocity" derived from our ex-
 186 pression for streamfunction shown in Equation 2:

$$V = -g \frac{d\Psi}{dp} \quad (3)$$

187 V represents the flow from low to high CRH area fractions, where negative values
 188 represent a return flow from high CRH values to low CRH values. Because the shallow
 189 circulation is characterized by a strong return flow, we use the strength of this return
 190 flow to represent the strength of the shallow circulation. Strong negative values repre-
 191 sent a strong return flow and strong shallow circulation. We calculate this index by find-
 192 ing the minimum of V below 500 hPa for each CRH value and taking the average across
 193 the full CRH range. This quantity is shown in Figure 3b for each case plotted against
 194 SST range. As in Figure 3a, each line represents a different global mean SST. The strength
 195 of the return flow increases with both mean SST and SST range. This figure specifically
 196 highlights that warming the SST, without increasing the SST gradient, increases the re-
 197 turn flow and shallow circulation strength. For the coldest case, the return flow strength
 198 only increases at the highest SST range, 15 K. In experiments with already strong shal-
 199 low circulation strength, such as F303.5-7.5, increasing either the mean SST or SST range
 200 appears to have diminishing effects on the return flow associated with the shallow cir-
 201 culation. Increasing either the SST range or warming the mean SST strengthens the shal-
 202 low circulation, and the strongest shallow circulations occur in experiments with both
 203 warm mean SSTs and large SST ranges.

204 Although we are characterizing these experiments by their mean SST and their SST
 205 range, it is important to note that changing either the mean SST or the SST range will
 206 also change the maximum SST. The maximum SST is particularly important in the trop-
 207 ics, as the tropospheric air temperature is primarily set by the warmest SSTs (Sobel et
 208 al., 2001).

209 Figure 4 shows the same index for shallow circulation strength used in Figure 3 plot-
 210 ted against the maximum SST for each experiment. The return flow strengthens with
 211 maximum SST. The strong and consistent dependence of shallow return flow on the max-
 212 imum SST suggests that the shallow circulation is related to the vertical profile of tem-
 213 perature and humidity of the atmosphere, which is controlled by the warmest temper-
 214 atures in the tropics.

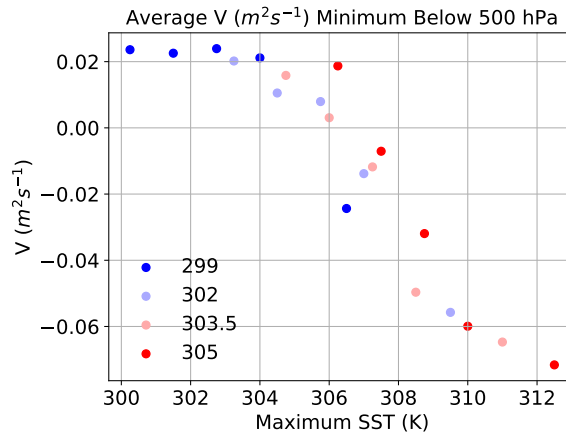


Figure 4. Minimum horizontal area velocity (V) averaged over all CRH values for each mean temperature, plotted against maximum SST. Global mean SST is represented by color.

215 3.2 Relative Humidity

216 The relative humidity is closely tied to both the circulation and the potential mech-
 217 anisms that drive it. Figure 5 shows contours of relative humidity (%) in pressure ver-
 218 sus CRH area fraction. An interesting feature of the relative humidity distribution is a
 219 deep secondary moist layer above the near-surface boundary layer. This layer is capped
 220 by a sharp transition to much drier air on a surface that slopes downward from the moist
 221 to the driest part of the domain. This layer becomes thinner and more moist as the SST
 222 gradient is increased. Although these models are highly idealized, this middle tropospheric
 223 moist layer can be found in observations and reanalysis data. A more detailed descrip-
 224 tion of this secondary moist layer in reanalysis data can be found in the Supplementary
 225 Material (Figure S3).

226 Later we will show enhanced shallow convection at temperatures just less than the
 227 maximum SST in our simulations. This shallow convection increases in strength with
 228 the mean SST, driving stronger shallow circulations in a warmed climate. We will then
 229 propose an analogy between the shallow convection that drives the shallow circulations
 230 in our experiments and the shallow convection that occurs in nature in regions of the trop-
 231 ics whose SST is slightly less than the tropical maximum.

232 Increasing the mean SST and increasing the SST gradient have different effects on
 233 the distribution of relative humidity. When increasing the SST range (bottom to top in
 234 Figure 5), the subsiding region dries and expands into higher CRH regions. This dry-
 235 ing effect is particularly noticeable for the range of CRH area fraction from 0.6-0.8. For
 236 any given global mean SST, increasing the SST range consistently dries out the mid tro-
 237 posphere (around 600 to 400 hPa) in this CRH window. However, warming the global
 238 mean SST while maintaining the same SST contrast has the opposite effect. Warming
 239 moistens the layer between 800 to 400 hPa in the window from 0.6 to 0.8 CRH area frac-
 240 tion.

241 The moistening or drying of the 0.6-0.8 CRH window has important effects for ra-
 242 diative cooling and convection. If the air above the boundary layer moistens (dries), long-
 243 wave cooling of the layer below can be suppressed (enhanced) (Hartmann et al., 2022;
 244 Jeevanjee & Fueglistaler, 2020). Conversely, if the air above the boundary layer dries (moist-
 245 ens), convection is suppressed (enhanced). So, the change in relative humidity in this CRH
 246 window indicates which mechanism is playing a more active role in strengthening the shal-

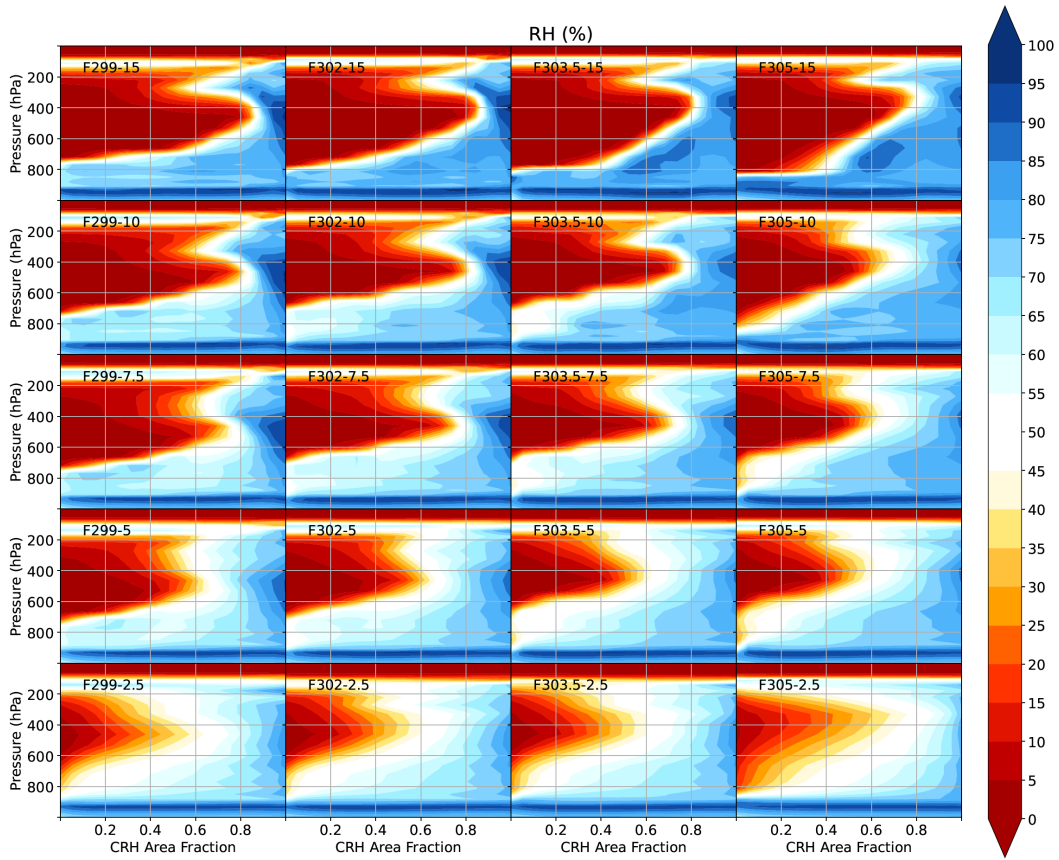


Figure 5. Relative humidity (%) for each case shown in pressure (hPa) and column relative humidity (CRH) area space (%). The global mean SST of each case increases from left to right, and the SST range increases from bottom to top.

247 low circulation. When increasing the SST range and drying this CRH window, the con-
 248 ditions are more favorable for longwave cooling. When warming the mean SST and moist-
 249 ening this CRH window, the conditions are more favorable for shallow convection. It is
 250 relevant to note here that the relative humidity and these mechanisms feed back on each
 251 other, so it is difficult to know which initially triggers the feedback loop. We will dis-
 252 cuss in more detail the effect of relative humidity on longwave cooling in Section 4 and
 253 on shallow convection in Section 5.

254 4 Boundary Layer Longwave Cooling

255 The longwave cooling above the boundary layer in the subsiding region is known
 256 to be strongly connected to the shallow circulation strength (Nolan et al., 2007). This
 257 relationship is characterized by a feedback between the longwave cooling and the shal-
 258 low circulation strength through effects on the column relative humidity. As the shal-
 259 low circulation strengthens, the troposphere of the subsiding region dries and the wa-
 260 ter vapor above the boundary layer decreases. Decreasing the water vapor path above
 261 the emission level leads to an increase in longwave cooling (Hartmann et al., 2022; Jee-
 262 vanjee & Fueglistaler, 2020). This increase in boundary layer longwave cooling in turn
 263 strengthens the shallow circulation (Nolan et al., 2007). Fildier et al. (2023) similarly
 264 find the vertical moisture distribution to have a significant role in the long-wave cool-

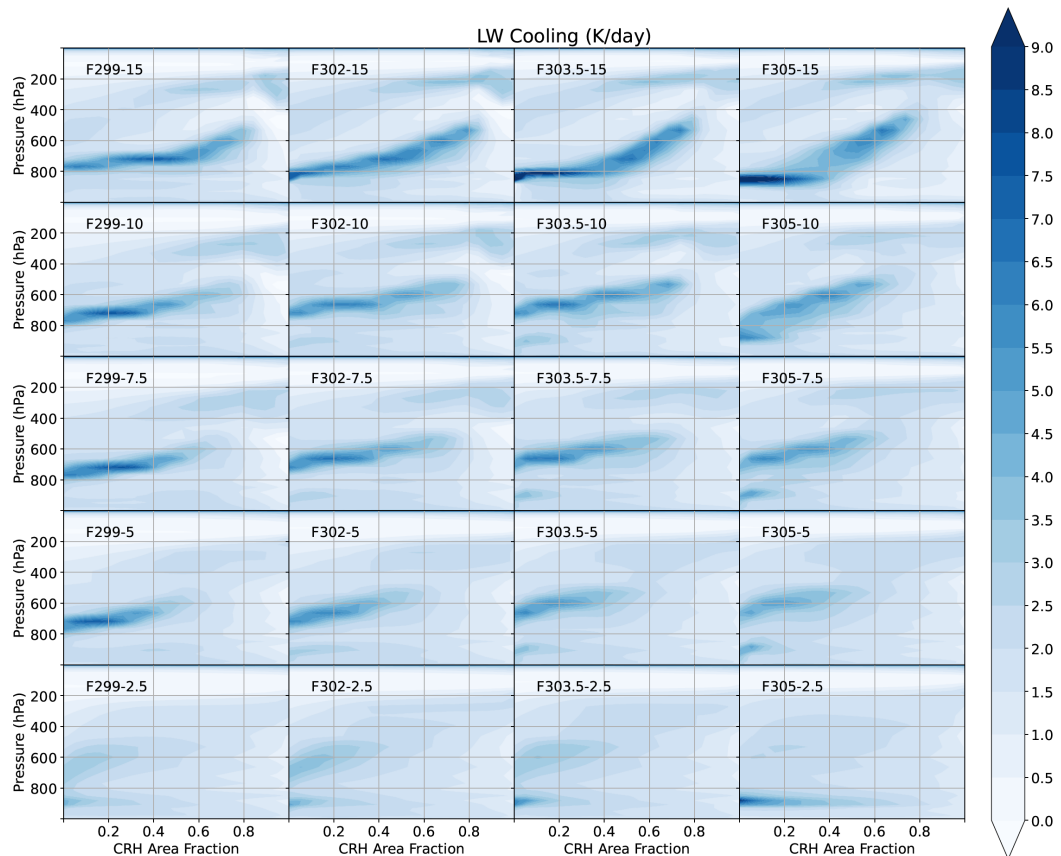


Figure 6. Longwave cooling (K/day) for each case shown in pressure (hPa) and column relative humidity (CRH) area space (%). The global mean SST of each case increases from left to right, and the SST range increases from bottom to top.

265 ing of the boundary layer, and specifically highlight the importance of moist intrusions
266 from remote convection in setting the humidity above the boundary layer.

267 As shown in Figure 6, for a given global mean SST, as the SST range increases, the
268 magnitude of the longwave cooling also increases. The band of enhanced longwave cool-
269 ing above the moist layer also expands into the intermediate region between subsidence
270 and deep convection with higher CRH. This enhancement in longwave cooling corresponds
271 to increasing shallow circulation strength, as expected. In summary, we find that the long-
272 wave cooling above the boundary layer tends to respond more strongly to an increase
273 in SST range rather than mean SST. This can largely be explained by the relative hu-
274 midity distribution.

275 The strength of longwave cooling is directly proportional to the amount of water
276 vapor above the emission level (Hartmann et al., 2022; Jeevanjee & Fueglistaler, 2020;
277 Fildier et al., 2023). Following Hartmann et al. (2022), the cooling-to-space approxima-
278 tion for the longwave cooling rate at a specified emission level and wavelength, λ is a func-
279 tion of its temperature and humidity at that level as well as the vapor pressure path above
280 that level

$$\frac{dT}{dt}|_{\bar{\lambda}} \approx -\left[\frac{\pi g}{C_p e} RHe_s(T) B_{\bar{\lambda}}\right] VPP^{-1} \quad (4)$$

281 where $B_{\bar{\lambda}}(T)$ is the Planck function, $e_s(T)$ is the saturation vapor pressure, C_p is the spe-
282 cific heat at constant pressure, and

$$VPP = \int_0^p RHe_s(T) dp \quad (5)$$

283 From this expression, we see that the longwave cooling is stronger when the vapor pres-
284 sure at the emission level is high and the vapor pressure path above the level of emis-
285 sion is small. Figure 7 shows (a) the longwave cooling, (b) the humidity component of
286 the cooling to space approximation shown above by (5), (c) the temperature profile, and
287 (d) the relative humidity profile for cases with a mean SST of 303.5 K and the full range
288 of SST gradients. Line plots versus pressure are shown for the CRH range of 0.6 to 0.8.
289 As described in Section 3.1, the strength of the shallow circulation corresponds to an ex-
290 pansion of the shallow cell to higher CRH area fraction values. Specifically, we identi-
291 fied the CRH area fraction from 0.6-0.8 as showing particularly distinct differences be-
292 tween warming and increasing the SST range. So, to analyze the mechanism responsi-
293 ble for this strengthening, we show averages over 0.6-0.8 CRH area fractions. We show
294 experiments with an SST of 303.5 K as a representative example of the changes with in-
295 creasing SST range.

296 Figure 7a shows the longwave cooling rates averaged from 0.6 to 0.8 CRH area frac-
297 tion in pressure coordinates. For this SST and CRH window, the longwave cooling peaks
298 at 532 hPa. Figure 7b shows a peak in $RHe_s(T)VPP^{-1}$ at the same pressure level, in-
299 dicating strong control of the vapor column on the longwave cooling. The VPP profile
300 peak is a combined effect of both moistening below the emission level and drying above.
301 In addition, because of the large-scale circulation and the weak temperature gradient in
302 the tropics, the temperature of the free troposphere of the entire tropics is set by the warmest
303 region. Figure 7c shows the temperature profiles for each SST range. As the SST range
304 increases, the air temperature increases, and there is a corresponding increase in emis-
305 sion temperature, and thus an increase to the longwave cooling. Because the temper-
306 ature and consequently the saturation vapor pressure increase with SST range, the re-
307 duction in VPP must be dominated by the decrease in relative humidity, shown in Fig-
308 ure 7d.

309 The VPP above the boundary layer in the subsiding region decreases with increas-
310 ing SST range. Because the longwave cooling is inversely proportional to the VPP, the
311 longwave cooling is then enhanced with increasing SST gradient. Because the longwave
312 cooling impacts the shallow circulation strength, which in turn impacts the drying above

313 the boundary layer, it is difficult to say whether one causing the other. However, there
314 is a clear trend in the changes in longwave cooling and VPP across changing SST dis-
315 tributions.

316 In these experiments, increasing the SST range strengthens the large-scale circu-
317 lation, which dries the mid troposphere in the subsiding region, and increases longwave
318 cooling. So, following the initial drying from the increase in SST range, we see a feed-
319 back between the longwave cooling, shallow circulation strength, and humidity of the sub-
320 siding region:

- 321 1. Drying the subsiding region strengthens the longwave cooling above the bound-
322 ary layer.
- 323 2. Longwave cooling strengthens the shallow circulation.
- 324 3. Moisture transport away from the subsiding region is enhanced, and the vapor pres-
325 sure above the boundary layer decreases.

326 Although the feedback described above begins with an increase in SST range strength-
327 ening subsidence drying in the free troposphere, because the SST in these experiments
328 is fixed, the circulation changes cannot feedback onto the SST range. In tropical RCE
329 experiments run with interactive SST, the SST distribution oscillates with a speed de-
330 pendingent on the mixed layer depth (Coppin & Bony, 2017, 2018; Dygert & Hartmann,
331 2023). In this study, we focus instead on the circulation response to an increase in SST
332 range.

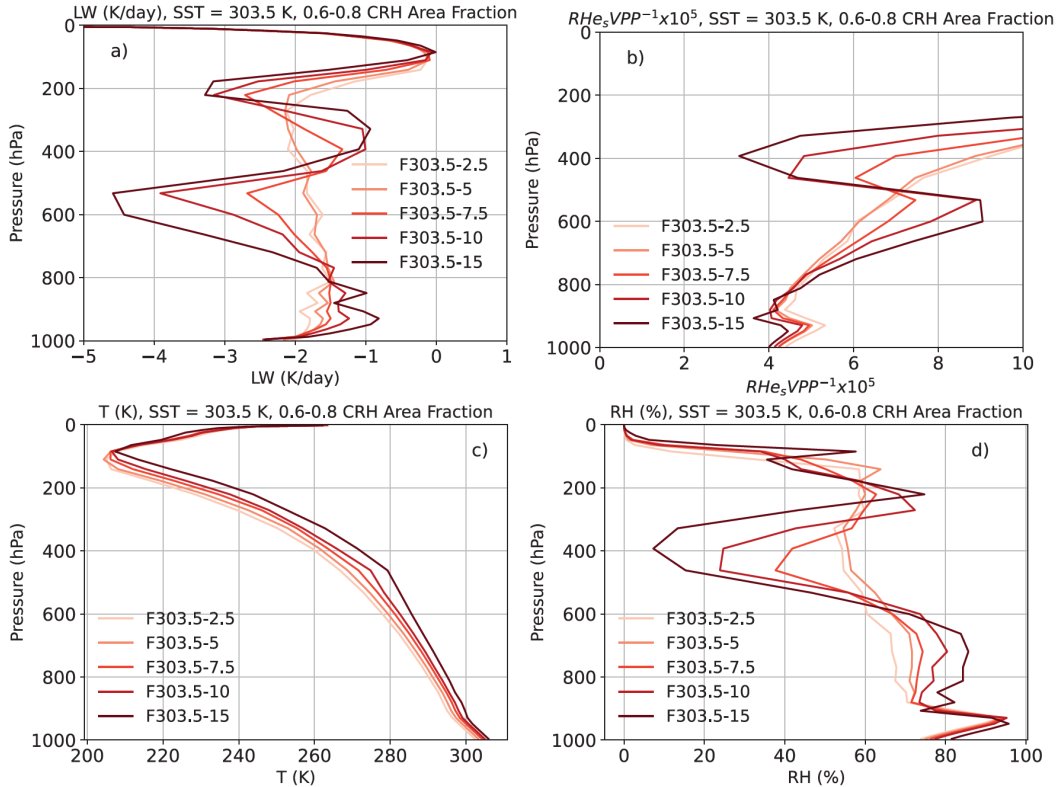


Figure 7. These panels show vertical profiles of quantities corresponding to experiments of each SST range with an SST of 303.5, averaged over 0.6-0.8 CRH area fraction. Panel (a) shows the temperature tendency from longwave cooling (K/day), (b) shows the humidity component of the longwave cooling approximation, $RHe_s(T)VPP^{-1}$, (c) temperature (K), and (d) relative humidity (%).

333

5 Shallow Convection

334 The longwave cooling of the moist layer provides a good consistency argument for
 335 the increasing shallow circulation with increasing SST gradient, but this longwave cool-
 336 ing does not work as well in understanding the increase in shallow circulation strength
 337 with increasing global mean SST. For a given SST range in Figure 6, as the global mean
 338 SST increases, the longwave cooling does not correspond as strongly with the increase
 339 in shallow circulation strength with mean SST. We also do not see the same expansion
 340 of peak longwave cooling into the intermediate region with increasing mean SST. We know
 341 from the streamfunctions shown in Figure 2 that the shallow cell strengthens and expands
 342 with increasing global mean SST. Because the longwave cooling does not strengthen and
 343 expand in this region with warming, an alternative explanation for the strengthening of
 344 the shallow cell with warming is required.

345 In this section we explore the role of shallow convection in driving stronger shal-
 346 low circulations as the mean SST is increased. Figure 8 shows the total heating from pa-
 347 rameterized convection in each case. For a given global mean SST, increasing the SST
 348 range does increase the strength of both deep and shallow convection, but the convec-
 349 tion occupies a narrow region, and does not expand into intermediate regions. When in-
 350 creasing the global mean SST, the shallow convection both intensifies and expands, moist-
 351 ening the mid troposphere over intermediate regions of CRH and SST.

352 The increase in shallow convection over intermediate SSTs also corresponds to an
 353 increase in relative humidity in the layer. To better understand how the increase in shal-
 354 low convection relates to humidity and sea surface temperature, we use a simplified model.
 355 Zhou and Xie (2019) use a spectral plume model (SPM) to illustrate the effect of entrain-
 356 ment on lapse rate. This model computes the effect of entrainment on the temperature
 357 of parcels rising in an unsaturated environment. The strength of the entrainment is con-
 358 trolled by a parameter, ϵ , which we set to $.3\text{ km}^{-1}$, which generates temperature pro-
 359 files that best fit our model data and is also the value chosen by Zhou and Xie (2019)
 360 to best fit the observed tropical temperature profile. We use this model to generate par-
 361 cel profiles for varying relative humidity profiles and sea surface temperatures. We then
 362 use these parcel profiles to calculate the convective available potential energy (CAPE),
 363 which we expect will explain the location of the shallow convection. Using this simpli-
 364 fied model allows us to look at the impact of entrainment drying on convection height,
 365 and how this height is influenced by relative humidity.

366 The total CAPE is defined as

$$367 \text{CAPE} = \int \frac{T_{v,p} - T_{v,env}}{T_{v,env}} dz \quad (6)$$

368 where $T_{v,p}$ is the parcel virtual temperature (generated by the SPM) and $T_{v,env}$ is the
 369 background virtual temperature (from the GCM data). In model coordinates, this can
 be written as

$$370 \text{CAPE} = \sum_i \frac{T_{v,p,i} - T_{v,env,i}}{T_{v,env,i}} \Delta z_i = \sum_i B_i \Delta z_i \quad (7)$$

371 We call the $B_i \Delta z_i$ at each model level the contribution to CAPE by that layer, and look
 372 at how the vertical distribution of this quantity changes from case to case and how this
 depends on the relative humidity distribution.

373 The top row of Figure 9 shows some test cases to illustrate the role of relative hu-
 374 midity on the vertical profile of CAPE contributions $B_i \Delta z_i$. Shown in green in Figure
 375 9a is the relative humidity in the 0.6-0.8 CRH band for the case F303.5-7.5. In addition,
 376 we show test profiles that have a maximum RH of 20, 40 and 80% above the 849 hPa
 377 level. The CAPE contributions calculated with the SPM model for these examples are
 378 shown in Figure 9b. Decreasing the relative humidity above 849 hPa relative to the model
 379 profile produces a sharp increase of CAPE just above 849 hPa, but this increase is very

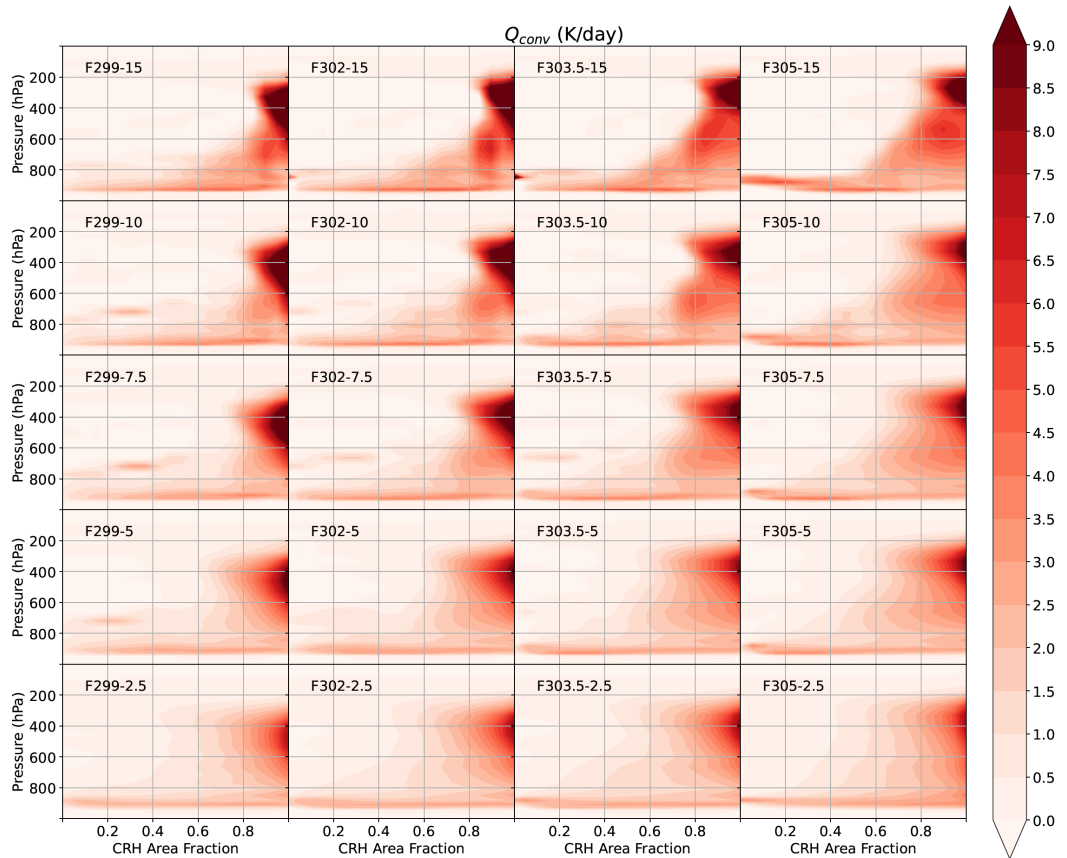


Figure 8. Heating from convection (K/day) for each case shown in pressure (hPa) and column relative humidity (CRH) area space (%). The global mean SST of each case increases from left to right, and the SST range increases from bottom to top.

380 shallow. This shallow CAPE increase is due to the effect of humidity on virtual temperature.
 381 The plume is assumed to be saturated, but the environment is assumed to have
 382 the prescribed RH profile. The dry RH profile decreases the virtual temperature of the
 383 environment, and so the buoyancy of the saturated parcel increases. This spike in buoy-
 384 ancy is very shallow and above about 750 hPa the CAPE contribution for these dry cases
 385 is less than the control case represented by the model. Lifted parcels experience a larger
 386 lapse rate when lifted in the drier environment, quickly leading to a colder parcel tem-
 387 perature, and thus reducing the buoyancy of the parcel.

388 On the other hand, the SPM predicts a deeper layer of positive CAPE contribu-
 389 tion for the moister 80% minimum RH case shown in Figure 9b. Parcels lifted into a moister
 390 environment maintain their buoyancy better and lead to increase CAPE contributions.

391 Figure 9 shows how the CAPE responds to warming in cases with a fixed SST con-
 392 trast of 7.5 K. Figure 9c shows that the heating from convection in the 800 to 600 hPa
 393 layer increases as the temperature is increased from 299 K to 305 K, consistent with stronger
 394 driving of a shallow circulation by shallow convection as the temperature increases. Fig-
 395 ure 9d shows that the plume model CAPE predicts this increase in shallow convection,
 396 since the layer of positive CAPE increases and deepens with increasing SST.

397 Although the magnitude of this effect is sensitive to the entrainment parameter used,
 398 the overall effect is consistent: drying limits the height convection reaches, and conversely,
 399 moistening can increase the height convection reaches. This is consistent with previous
 400 work investigating the impact of environmental humidity on convection (Derbyshire et
 401 al., 2004). There is, however, a limit to how much increasing the relative humidity can
 402 increase the height of convection. Shown in Figure 9b and d, there is a consistent, sharp
 403 decline in CAPE contribution around 500 hPa. As the temperature decreases at higher
 404 altitudes, the saturation specific humidity decreases, and its effect on the buoyancy and
 405 virtual temperature is reduced. Similarly, the effect of drying on the convection height
 406 is stronger at lower altitudes where the atmosphere is warmer and specific humidity has
 407 a larger impact on the buoyancy.

408 Janssens et al. (2024) find shallow convection to be the primary driver of mesoscale
 409 shallow circulations, and also note that the SST range in the circulations considered is
 410 small. Although the mechanisms governing the relationship between convection and cir-
 411 culation may differ between spatial scales (Tomassini, 2020), we find a similar relation-
 412 ship at a much larger scale. Here, we find that shallow convection plays a significant role
 413 when warming the global mean SST, and increasing the SST range can actually limit
 414 the impact of shallow convection through the drying of the mid troposphere above the
 415 moist layer. Dry mid tropospheres strengthen longwave cooling, while moister mid tro-
 416 pospheres favor shallow convection. Shallow convection also brings moisture up from the
 417 surface and increases the humidity, making the environment more favorable for future
 418 shallow convection.

419 In these experiments, increasing the global mean SST increases shallow CAPE in
 420 the intermediate region between subsidence and deep convection, and this leads to an
 421 increase in shallow convection. The moistening and extension of the lower tropospheric
 422 moist layer with a warming climate can be clearly seen in the relative humidity sections
 423 in Figure 5. A feedback process between shallow convection and relative humidity works
 424 as follows:

- 425 1. Shallow convection strengthens and enhances the secondary moist layer.
- 426 2. A moist lower free troposphere favors shallow convection.

427 This process becomes stronger with warming as shallow CAPE increases with a warm-
 428 ing climate.

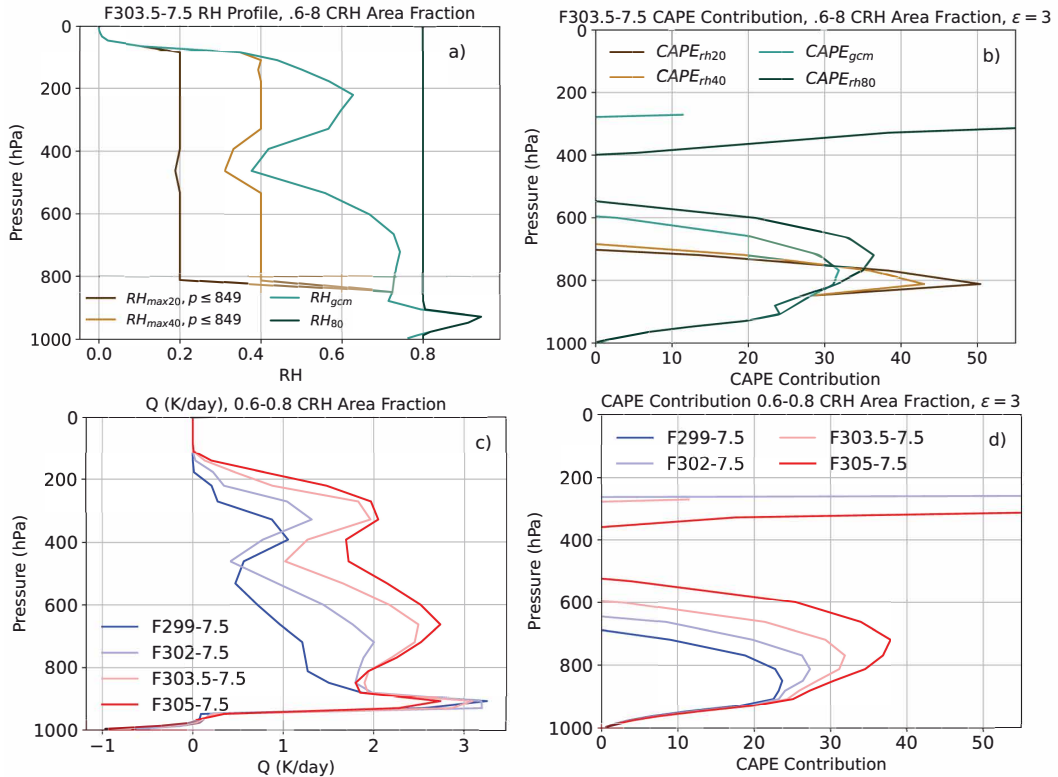


Figure 9. The top row shows the CAPE dependence on relative humidity. Panel a shows the relative humidity profiles used to generate parcel profiles in the SPM, (b) the CAPE contribution for each relative humidity profile. The bottom row shows the CAPE dependence on mean SST. Panel c shows the heating from convection (K/day), panel d shows the CAPE contribution for cases with a range of 7.5 K.

429 **6 Summary**

430 Tropical shallow circulations are significant in both observations and in idealized
 431 modeling experiments. Potential drivers for shallow circulation strength include bound-
 432 ary layer pressure gradients driven by sea surface temperature distributions, boundary
 433 layer longwave cooling, and shallow convection. Here, we use an idealized model to look
 434 at the relationship between the sea surface temperature gradient, mean sea surface tem-
 435 perature magnitude, and the shallow circulation strength.

436 We find that different drivers dominate depending on whether we increase the SST
 437 range or increase the global mean SST. In both cases, this strengthening of the shallow
 438 cell corresponds to anomalous heating rates above the boundary layer. When increas-
 439 ing the SST range, the longwave cooling above the boundary layer in the dry, subsid-
 440 ing region increases as the shallow circulation strengthens. When increasing the global
 441 mean SST, the shallow convection over intermediate CRH/SSTs increases, but there is
 442 not a strong increase in the longwave cooling above the boundary layer. In summary,
 443 increasing the SST range strengthens the shallow circulation by increasing the longwave
 444 cooling rate, while increasing the global mean SST strengthens the shallow circulation
 445 by increasing the shallow convection over intermediate SSTs.

- 446 • When increasing the SST range, the boundary layer longwave cooling increases
 447 as both the deep and shallow circulations strengthen and the subsiding region dries.
- 448 • When increasing the global mean SST, heating from shallow convection dominates.
 449 An increase in CAPE over the intermediate region between deep convection and
 450 subsidence leads to an increase in shallow convection, moistening the mid tropo-
 451 sphere and making the environment more favorable for further convection.
- 452 • The conditions favorable for each mechanism work in opposition to each other.
 453 Drying above the boundary layer leads to an increase in longwave cooling, but is
 454 less favorable for shallow convection due to effects from entrainment drying. Con-
 455 versely, moistening above the boundary layer is more favorable for shallow con-
 456 vention, but limits the longwave cooling.

457 These idealized experiments present a simplified, qualitative relationship between
 458 these mechanisms and are thus limited in their application to a more realistic setting.
 459 For example, the relative humidity in the subsiding region is often much drier than would
 460 be expected from observations. This may over-emphasize the significance of entrainment
 461 drying on convection. In scenarios with moister subsiding regions, convergence forced
 462 shallow convection could play a larger role when increasing the SST gradient, as in Back
 463 and Bretherton (2009). Similarly, we use the quantity CAPE in an attempt to connect
 464 our results to a quantity applicable to observations, but in our model convection is pa-
 465 rameterized. Despite these limitations, these results provide a useful framework for the
 466 indirect effect of SST on shallow circulation.

467 **7 Open Research**

468 The model used is Geophysical Fluid Dynamics Laboratory's (GFDL) AM2.1 (Anderson
 469 et al., 2004). ERA5 variables are downloaded from the main database (Copernicus Cli-
 470 mate Change Service, 2022). Data and code supporting figures can be found at https://github.com/bdygert/shallow_circulation (Dygert & Hartmann, 2025).

472 **8 Conflict of Interest Statement**

473 The authors have no conflicts of interest to disclose.

474 **Acknowledgments**

475 This work was supported by NSF Grant AGS-2124496. We thank the reviewers for their
 476 helpful comments and suggestions.

477 **References**

478 Anderson, J., Broccoli, A., Cooke, W., Delworth, T., Dixon, K., Donner, L., ...
 479 Garner, S. (2004). The new GFDL global atmosphere and land model
 480 AM2-LM2: Evaluation with prescribed SST simulations. *Journal of Climate*,
 481 17(24), 4641–4673. doi: 10.1175/jcli-3223.1

482 Armour, K. C., Proistosescu, C., Dong, Y., Hahn, L. C., Blanchard-Wrigglesworth,
 483 E., Pauling, A. G., ... Gregory, J. M. (2024). Sea-surface temperature pattern
 484 effects have slowed global warming and biased warming-based constraints on
 485 climate sensitivity. *Proceedings of the National Academy of Sciences*, 121(12).
 486 doi: 10.1073/pnas.2312093121

487 Back, L. E., & Bretherton, C. S. (2009). On the relationship between SST gradi-
 488 ents, boundary layer winds, and convergence over the tropical oceans. *Journal*
 489 *of Climate*, 22(15), 4182–4196. doi: 10.1175/2009jcli2392.1

490 Bony, S., Stevens, B., Frierson, D. M. W., Jakob, C., Kageyama, M., Pincus, R.,
 491 ... Webb, M. J. (2015). Clouds, circulation and climate sensitivity. *Nature*
 492 *Geoscience*, 8(4), 261–268. doi: 10.1038/ngeo2398

493 Copernicus Climate Change Service. (2022). *Mass-consistent atmospheric energy*
 494 *and moisture budget monthly data from 1979 to present derived from era5 re-*
 495 *analysis*. ECMWF. Retrieved from <https://cds.climate.copernicus.eu/>
 496 doi/10.24381/cds.c2451f6b doi: 10.24381/CDS.C2451F6B

497 Coppin, D., & Bony, S. (2017). Internal variability in a coupled general circula-
 498 tion model in radiative-convective equilibrium. *Geophysical Research Letters*,
 499 44(10), 5142–5149. Retrieved from <http://dx.doi.org/10.1002/2017GL073658> doi: 10.1002/2017gl073658

500 Coppin, D., & Bony, S. (2018). On the interplay between convective aggregation,
 501 surface temperature gradients, and climate sensitivity. *Journal of Advances in*
 502 *Modeling Earth Systems*, 10(12), 3123–3138. Retrieved from <http://dx.doi.org/10.1029/2018MS001406> doi: 10.1029/2018ms001406

503 Derbyshire, S. H., Beau, I., Bechtold, P., Grandpeix, J., Piriou, J., Redelsperger, J.,
 504 & Soares, P. M. M. (2004). Sensitivity of moist convection to environmental
 505 humidity. *Quarterly Journal of the Royal Meteorological Society*, 130(604),
 506 3055–3079. Retrieved from <http://dx.doi.org/10.1256/qj.03.130> doi:
 507 10.1256/qj.03.130

508 Dong, Y., Proistosescu, C., Armour, K. C., & Battisti, D. S. (2019). Attribut-
 509 ing historical and future evolution of radiative feedbacks to regional warming
 510 patterns using a green's function approach: The preeminence of the western
 511 pacific. *Journal of Climate*, 32(17), 5471–5491. doi: 10.1175/jcli-d-18-0843.1

512 Dygert, B. D., & Hartmann, D. L. (2023). The cycle of large-scale aggregation
 513 in tropical radiative-convective equilibrium. *Journal of Geophysical Re-*
 514 *search: Atmospheres*, 128(7). Retrieved from <http://dx.doi.org/10.1029/2022JD037302> doi: 10.1029/2022jd037302

515 Dygert, B. D., & Hartmann, D. L. (2025). *Effects of sea surface temperature on*
 516 *shallow circulation strength* [Dataset]. Retrieved from https://github.com/bdygert/shallow_circulation (model data)

517 Fildier, B., Muller, C., Pincus, R., & Fueglistaler, S. (2023). How moisture shapes
 518 low-level radiative cooling in subsidence regimes. *AGU Advances*, 4(3). doi: 10
 519 .1029/2023av000880

520 Fläschner, D., Mauritsen, T., Stevens, B., & Bony, S. (2018). The signature
 521 of shallow circulations, not cloud radiative effects, in the spatial distribu-
 522 tion of tropical precipitation. *Journal of Climate*, 31(23), 9489–9505. doi:
 523 10.1029/2018JD029000

527 10.1175/jcli-d-18-0230.1

528 Grabowski, W. W., Yano, J.-I., & Moncrieff, M. W. (2000). Cloud resolv-
529 ing modeling of tropical circulations driven by large-scale SST gradi-
530 ents. *Journal of the Atmospheric Sciences*, 57(13), 2022–2040. doi:
531 10.1175/1520-0469(2000)057<2022:crmotc>2.0.co;2

532 Hartmann, D. L., & Dygert, B. D. (2022). Global radiative convective equilibrium
533 with a slab ocean: SST contrast, sensitivity and circulation. *Journal of Geo-
534 physical Research: Atmospheres*, 127(12). doi: 10.1029/2021jd036400

535 Hartmann, D. L., Dygert, B. D., Blossey, P. N., Fu, Q., & Sokol, A. B. (2022). The
536 vertical profile of radiative cooling and lapse rate in a warming climate. *Jour-
537 nal of Climate*, 35(19), 6253–6265. doi: 10.1175/jcli-d-21-0861.1

538 Hersbach, H., Bell, B., Berrisford, P., Hirahara, S., Horányi, A., Muñoz-Sabater, J.,
539 ... Thépaut, J. (2020). The era5 global reanalysis. *Quarterly Journal of the
540 Royal Meteorological Society*, 146(730), 1999–2049. doi: 10.1002/qj.3803

541 Huaman, L., Schumacher, C., & Sobel, A. H. (2022). Assessing the vertical veloc-
542 ity of the east pacific itcz. *Geophysical Research Letters*, 49(1). doi: 10.1029/
543 2021gl096192

544 Janssens, M., George, G., Schulz, H., Couvreux, F., & Bouniol, D. (2024). Shallow
545 convective heating in weak temperature gradient balance explains mesoscale
546 vertical motions in the trades. *Journal of Geophysical Research: Atmospheres*,
547 129(18). doi: 10.1029/2024jd041417

548 Jeevanjee, N., & Fueglistaler, S. (2020). On the cooling-to-space approx-
549 imation. *Journal of the Atmospheric Sciences*, 77(2), 465–478. doi:
550 10.1175/jas-d-18-0352.1

551 Knutson, T. R., & Manabe, S. (1995). Time-mean response over the tropical pa-
552 cific to increased c02in a coupled ocean-atmosphere model. *Journal of Climate*,
553 8(9), 2181–2199. doi: 10.1175/1520-0442(1995)008<2181:tmrott>2.0.co;2

554 Larson, K., & Hartmann, D. L. (2003). Interactions among cloud, water vapor,
555 radiation, and large-scale circulation in the tropical climate. part ii: Sensitivity
556 to spatial gradients of sea surface temperature. *Journal of Climate*, 16(10),
557 1441–1455. doi: 10.1175/1520-0442(2003)016<1441:IACWVR>2.0.CO;2

558 Lindzen, R. S., & Nigam, S. (1987). On the role of sea surface temperature gradients
559 in forcing low-level winds and convergence in the tropics. *Journal of the Atmo-
560 spheric Sciences*, 44(17), 2418–2436. doi: 10.1175/1520-0469(1987)044<2418:
561 otross>2.0.co;2

562 Lutsko, N. J., & Cronin, T. W. (2018). Increase in precipitation efficiency with sur-
563 face warming in radiative-convective equilibrium. *Journal of Advances in Mod-
564eling Earth Systems*, 10(11), 2992–3010. doi: 10.1029/2018ms001482

565 Lutsko, N. J., & Cronin, T. W. (2024). The transition to double-celled circulations
566 in mock-Walker simulations. *Geophysical Research Letters*, 51(14). doi: 10
567 .1029/2024gl108945

568 Moorthi, S., & Suarez, M. J. (1992). Relaxed Arakawa-Schubert. a parameteriza-
569 tion of moist convection for general circulation models. *Monthly Weather Re-
570 view*, 120(6), 978–1002. doi: 10.1175/1520-0493(1992)120<0978:rasapo>2.0.co;
571 2

572 Naumann, A. K., Stevens, B., Hohenegger, C., & Mellado, J. P. (2017). A con-
573 ceptual model of a shallow circulation induced by prescribed low-level radia-
574 tive cooling. *Journal of the Atmospheric Sciences*, 74(10), 3129–3144. doi:
575 10.1175/jas-d-17-0030.1

576 Nishant, N., Sherwood, S. C., & Geoffroy, O. (2016). Radiative driving of shallow
577 return flows from the itcz. *Journal of Advances in Modeling Earth Systems*,
578 8(2), 831–842. doi: 10.1002/2015ms000606

579 Nolan, D. S., Zhang, C., & Chen, S.-h. (2007). Dynamics of the shallow meridional
580 circulation around intertropical convergence zones. *Journal of the Atmospheric
581 Sciences*, 64(7), 2262–2285. doi: 10.1175/jas3964.1

582 Schulz, H., & Stevens, B. (2018). Observing the tropical atmosphere in moisture
583 space. *Journal of the Atmospheric Sciences*, 75(10), 3313–3330. doi: 10.1175/
584 jas-d-17-0375.1

585 Sobel, A. H., & Neelin, J. D. (2006). The boundary layer contribution to intertrop-
586 ical convergence zones in the quasi-equilibrium tropical circulation model
587 framework. *Theoretical and Computational Fluid Dynamics*, 20(5–6), 323–350.
588 doi: 10.1007/s00162-006-0033-y

589 Sobel, A. H., Nilsson, J., & Polvani, L. M. (2001). The weak temperature gradi-
590 ent approximation and balanced tropical moisture waves. *Journal of the Atmo-
591 spheric Sciences*, 58(23), 3650–3665. doi: 10.1175/1520-0469(2001)058<3650:
592 twtgaa>2.0.co;2

593 Tokioka, T., Yamazaki, K., Kitoh, A., & Ose, T. (1988). The equatorial 30–60 day
594 oscillation and the Arakawa-Schubert penetrative cumulus parameterization.
595 *Journal of the Meteorological Society of Japan. Ser. II*, 66(6), 883–901. doi:
596 10.2151/jmsj1965.66.6.883

597 Tomassini, L. (2020). The interaction between moist convection and the atmo-
598 spheric circulation in the tropics. *Bulletin of the American Meteorological Soci-
599 ety*, 101(8), E1378–E1396. doi: 10.1175/bams-d-19-0180.1

600 Vecchi, G. A., & Soden, B. J. (2007). Global warming and the weakening of the
601 tropical circulation. *Journal of Climate*, 20(17), 4316–4340. doi: 10.1175/
602 jcli4258.1

603 Yano, J.-I., Grabowski, W. W., & Moncrieff, M. W. (2002). Mean-state convective
604 circulations over large-scale tropical SST gradients. *Journal of the Atmospheric
605 Sciences*, 59(9), 1578–1592. doi: 10.1175/1520-0469(2002)059<1578:msccol>2.0
.co;2

607 Zhang, C., McGauley, M., & Bond, N. A. (2004). Shallow meridional circulation in
608 the tropical Eastern Pacific. *Journal of Climate*, 17(1), 133–139. doi: 10.1175/
609 1520-0442(2004)017<0133:smcitt>2.0.co;2

610 Zhang, C., Nolan, D. S., Thorncroft, C. D., & Nguyen, H. (2008). Shallow merid-
611 ional circulations in the tropical atmosphere. *Journal of Climate*, 21(14),
612 3453–3470. doi: 10.1175/2007jcli1870.1

613 Zhou, W., & Xie, S.-P. (2019). A conceptual spectral plume model for understand-
614 ing tropical temperature profile and convective updraft velocities. *Journal of
615 the Atmospheric Sciences*, 76(9), 2801–2814. doi: 10.1175/jas-d-18-0330.1